Resonant x-ray scattering study of magnetic and orbital order in $KCuF_3$

R. Caciuffo
Istituto Nazionale per la Fisica della Materia, Dipartimento di Fisica ed Ingegneria dei Materiali e del Territorio, Università di Ancona, Via Brecce Bianche, I-60131 Ancona, Italy

L. Paolasini and A. Sollier
European Synchrotron Radiation Facility, Boîte Postale 220, F-38043 Grenoble, France

P. Ghigna
Dipartimento di Chimica Fisica, Università di Pavia, I-27100 Pavia, Italy

E. Pavarini
Istituto Nazionale per la Fisica della Materia, Dipartimento di Fisica A. Volta, Università di Pavia, Via Bassi 6, I-27100 Pavia, Italy

J. van den Brink
Computational Materials Science and Mesa+ Research Institute, Faculty of Applied Physics, University of Twente, P.O. Box 217, 7500 AE Enschede, The Netherlands

M. Altarelli
Sincrotrone Trieste and Abdus Salam International Centre for Theoretical Physics, Trieste, Italy
(Received 24 January 2002; published 3 May 2002)

We present the results of resonant x-ray scattering experiments on $KCuF_3$. Structurally forbidden reflections, corresponding to magnetic and $3d$-orbital long-range order, have been observed. Integrated intensities have been measured as a function of incident energy, polarization, azimuthal angle, and temperature. By means of *ab initio* local spin density approximation (LSDA) and local spin density approximation with on-site Coulomb interaction (LSDA+U) calculations we determine the electronic structure of $KCuF_3$ and obtain the resonant x-ray scattering spectrum at the Cu K edge, which shows good agreement with the experimental data. Orbital and spin degrees of freedom are strongly coupled, and the temperature dependence of the intensity of orbital Bragg peaks reveals a correlation between magnetic and orbital order parameters.

DOI: 10.1103/PhysRevB.65.174425 PACS number(s): 75.30.Et, 71.30.+h, 71.90.+q, 71.70.−d

I. INTRODUCTION

A number of papers have been published during the last four decades dealing with the physical properties of the pseudocubic perovskite $KCuF_3$. This system belongs to a class of Mott-Hubbard insulators containing transition-metal ions whose magnetic behavior is largely determined by the structural configuration and the presence of nearly degenerate, partially occupied orbitals. The magnitude and sign of the superexchange interaction depend on the filling of the orbitals, and are therefore indeterminate in presence of degeneracy. The empirical Goodenough-Anderson-Kanamori rules,[1] for instance, cannot be applied if the type of occupied orbital is not known. The superexchange Hamiltonian must be generalized, to include the orbital degrees of freedom among with the spin ones. This was done almost thirty years ago by Kugel' and Khomskii (KK), who proposed a model able to describe the ordering of orbitals by superexchange in substances containing ions with orbital degeneracy, and to predict the corresponding magnetic structure.[2,3] The KK model shows that symmetry breaking, lifting, the electronic degeneracy, leads to magnetic and orbital long-range orders that are closely related, even if they occur at different temperatures.

$KCuF_3$ represents the simplest realization of a KK system. The Cu^{2+} ions have the $3d^9$ configuration, with completely filled t_{2g} orbitals and a single hole in the almost degenerate $3d_{x^2-y^2}$ and $3d_{3z^2-r^2}$ e_g states. The mean-field phase diagram and the dynamics of the KK Hamiltonian for the corresponding case of spins $S=1/2$ and doubly degenerate e_g states reproduce, qualitatively, the essential physics of $KCuF_3$.[4,5]

The crystal structure of $KCuF_3$ is made up of distorted CuF_6 octahedra, arranged in such a way as to give an almost equal Cu-Cu distance along the three principal axes of the pseudocubic perovskite cell ($a=b=8.2802$ Å, $c=7.852$ Å). The octahedral symmetry is broken, well above room temperature, by an orbital polarization accompanied by a Jahn-Teller (JT) cooperative distortion.[2,5] CuF_6 octahedra that are adjacent in the (**a**,**b**) plane are elongate along the **a** or **b** axis, and arranged in an antiferrodistortive pattern. If the squares of F ions superposed in neighboring (**a**,**b**) planes are rotated in opposite directions with respect to the undistorted configuration, the so-called *type-a* structure is realized, whereas the *type-d* arrangement is obtained if superposed F squares are rotated in the same sense.[6] In either case, the distortion corresponds to an alternate occupation of $3d_{x^2-z^2}$ and $3d_{y^2-z^2}$ hole states, i.e., to planes of perpendicularly oriented orbitals. Band-structure calculations using the local-density approximation (LDA) with the electron interactions treated in Hartree-Fock approximation (LDA+U method) support this picture.[7] According to the Goodenough-

Anderson-Kanamori rules, the orbital configuration results in nearest-neighbor superexchange interactions that are antiferromagnetic and strong along the **c** axis, ferromagnetic and weak in the (**a**,**b**) plane, as expressed by the ratio $|J_c|/J_a = 100$ between the nearest-neighbor superexchange interactions along and perpendicular to **c**.[8]

Indeed, above 38 K, $KCuF_3$ is a good realization of the one-dimensional antiferromagnetic (AF) nearest-neighbor Heisenberg model. The spin dynamics have been studied extensively and found to be in good agreement with the unbound spinon model.[9–11] Long-range three-dimensional AF order develops below $T_N = 38$ K for *type a*, and below 22 K for *type-d* structure; in both cases the magnetic propagation vector is $\langle 001 \rangle$ and the ordered moment is $\mu_0 = 0.48\mu_B$.[12] The crossover from one-dimensional to three-dimensional behavior is signaled by the appearance in the magnetic response of a longitudinal mode, the physical origin of which is the zero-point fluctuations that suppress the ordered moment in the coupled chain system.[13]

In this paper, we present the results of resonant x-ray scattering (RXS) experiments performed on good quality $KCuF_3$ single crystals. Structurally forbidden reflections, corresponding to magnetic and $3d$-orbital long-range order, have been observed. Integrated intensities have been measured as a function of temperature and incident-photon energy and polarization. The direction of the magnetic moment in the ordered phase and the symmetry of the orbitals have been determined from measurements of the Bragg intensity as a function the azimuthal angle around superlattice vectors. Nonresonant azimuthal scans about magnetic peaks were also performed to determine the angular momentum contribution to the magnetic moment. It appears that orbital and magnetic orderings are closely related, with a definite interplay between magnetic and orbital order parameters as revealed by an increase in the intensity of orbital Bragg peaks in the temperature range close to the Neél point. *Ab initio* local spin density approximation (LSDA) and local spin density approximation with on-site Coulomb interaction (LSDA+U) calculations are also presented. The calculated spectrum and azimuthal angle dependence at the Cu K edge reproduce the measured data without adjustable parameters.

II. EXPERIMENTAL METHOD AND DETAILS

RXS is due to a process in which a photon is virtually absorbed by exciting a core electron to empty states, and subsequently reemitted when the excited electron and the core hole recombine.[14–16] This process introduces anisotropic contributions to the x-ray susceptibility tensor,[17] the amplitude of which increases dramatically as the photon energy is tuned to an atomic absorption edge. In presence of long-range order of magnetic moments, electronic orbitals occupancy or spatially anisotropic valence-electron clouds, the interference of the anomalous anisotropic scattering amplitudes lead to the excitation of Bragg peaks at positions forbidden by the crystallographic space group. For absorbing atoms belonging to the transition-metal series, only the K edge may be of practical use, as the energy of other absorption edges is usually below the cut off for Bragg diffraction.

For the Cu K edge, the intermediate states involved are the $4p$ (electric dipole transitions) and the $3d$ (electric quadrupole transitions). The sensitivity of the experiment to magnetic order at the quadrupole, $1s$-$3d$, threshold energy has its origin in the spin polarization of the $3d$ states, whilst at the $1s$-$4p$ dipole transition energy the resonant enhancement for magnetic reflections is due to the $4p$-$3d$ intra-atomic Coulomb interaction and to the mixing of the $4p$ with the $3d$ states of neighboring Cu atoms.[18] The two resonant terms are superimposed to a much weaker, nonresonant contribution.[19,20] Both the resonant and the nonresonant magnetic scattering amplitudes depend on the polarization of the incident (σ, π) and of the scattered (σ', π') photons, and are discussed in Refs. 16,19,20.

RXS is also sensitive to the occupancy of $3d$ valence orbitals, and has been used to probe orbital long-range order in several manganites and transition-metal oxides.[21–25] Forbidden reflections become permitted due to the asphericity of the atomic electron density giving rise to an anomalous tensor component in the atomic scattering factor. In Mn perovskites, the resonant enhancement of superlattice reflections corresponding to orbital ordering have been observed by tuning the photon energy at the Mn K-absorption edge. Theoretical models suggest that the resonance is due to $1s \rightarrow 4p$ electric-dipole transitions, the splitting of the $4p$ states being mainly due to the JT distortion that accompanies the orbital ordering.[26–28]

The experiments have been performed on the ID20 beamline[29] of the European Synchrotron Radiation Facility (ESRF) in Grenoble, France. The spectrometer exploits the third-harmonic emission of a 42-mm-period undulator device. A double crystal Si(111) curved monochromator provides sagittal focusing and selects the appropriate x-ray energy. Vertical focusing and filtering of higher harmonics is achieved by Si mirrors that deliver at the sample position a 99% linearly polarized beam, with polarization perpendicular to the scattering plane (σ) and wave vector $\mathbf{k}_i$. The energy resolution is of 0.8 eV (full width at half maximum) at the Cu K edge. A mosaic crystal positioned between the sample and the detector is used to analyze whether the polarization of the scattered beam (with wave vector $\mathbf{k}_f$) is parallel (π') or perpendicular (σ') to the vertical scattering plane. A schematic representation of the experimental setup is shown in Fig. 1.

For resonant scattering experiments we operated the spectrometer around the Cu K edge of 8.995 keV, using the (004) reflection from a LiF analyzer (Bragg angle of 43.3° at the Cu K edge, no correction was performed to account for the departure from the ideal 45° orientation of the analyzer crystal). Non-resonant measurements were conducted at 5.218 and 7.828 keV, with (004) and (006) pyrolithic graphite analyzers, respectively (analyzer Bragg angle of 45°).

Single crystals of $KCuF_3$ have been prepared following the procedure described in Ref. 30. An aqueous solution of HF (45% in volume) was added to a suspension of $CuCO_3$ in a Teflon becker until a limpid solution was obtained. Then, a stoichiometric amount of an aqueous solution of KF was added, and the resulting limpid solution was kept still at room temperature. The slow evaporation of water yielded pale blue crystals of $KCuF_3$ of about $5 \times 5 \times 5$ mm^3 in size.

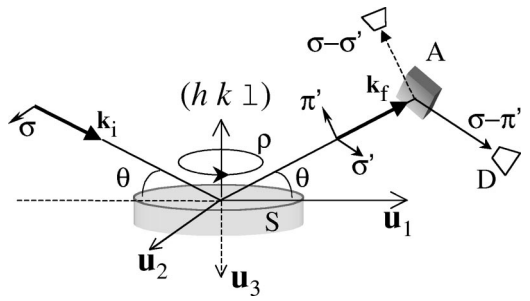

FIG. 1. Schematic representation of the experimental setup of the ESRF ID 20 beamline. A photon beam polarized perpendicularly to the (vertical) scattering plane impinges on the sample *S* and is scattered towards the analyzer crystal *A*. The scattered beam components with polarization parallel (π') or perpendicular (σ') to the scattering plane can be selected by an appropriate orientation of the analyzer. *D* is a standard scintillation detector. Integrated intensities of Bragg peaks are measured as a function of the photon energy for different values of the azimuthal angle ρ, defining the crystal orientation about the scattering vector (hkl). The unit vectors $\mathbf{u}_i$ define the reference frame.

Several crystals were cut to form either a (100) or a (110) flat clean surface, and carefully characterized by x-ray diffraction. Specimens with *type-d* regions extended over no more than a few percent of the entire volume were chosen for the experiments. The sample was mounted inside a closed-cycle refrigerator, allowing a base temperature of 10 K, with the vector normal to the clean surface lying in the scattering plane. Integrated intensities I_m were obtained numerically, by fitting a linear background and a Lorentzian line shape to the measured Bragg peaks. Corrections for the size of the footprint of the incident beam and for absorption were applied as $I_c = I_m \mu (1+\sin\alpha/\sin\beta)$, where α and β are the angles formed by the incident and scattered beam directions with the sample surface, and μ is the energy dependent absorption coefficient.

III. MAGNETIC SCATTERING

A. Resonant magnetic scattering

The appearance of resonant superlattice reflections with propagation vector $\langle 001 \rangle$ signals the occurrence of AF order below $T_N = 38$ K. The integrated intensity of the magnetic (441) Bragg peak is shown in Fig. 2, as a function of the photons energy, for both σ-σ' and σ-π' polarization channels. The fluorescence yield measured at 12 K is also shown, as an energy reference.

Two features are observed in the spectrum of the σ-π' component, one centered about the $1s \rightarrow 4p$ intra-atomic dipole transition, the other around the quadrupole $1s-3d$ threshold energy ($E_2 = 8.974$ keV). An antiresonant dip at the high-energy side of the quadrupolar peak is also visible. The complex structure of the resonance spectrum suggests a non-negligible hybridization between Cu $4p$ and fluorine orbitals.

The nonresonant behavior of the σ-σ' channel at the dipole edge confirms the magnetic origin of the measured signal. However, a weak quadrupolar resonance can be seen

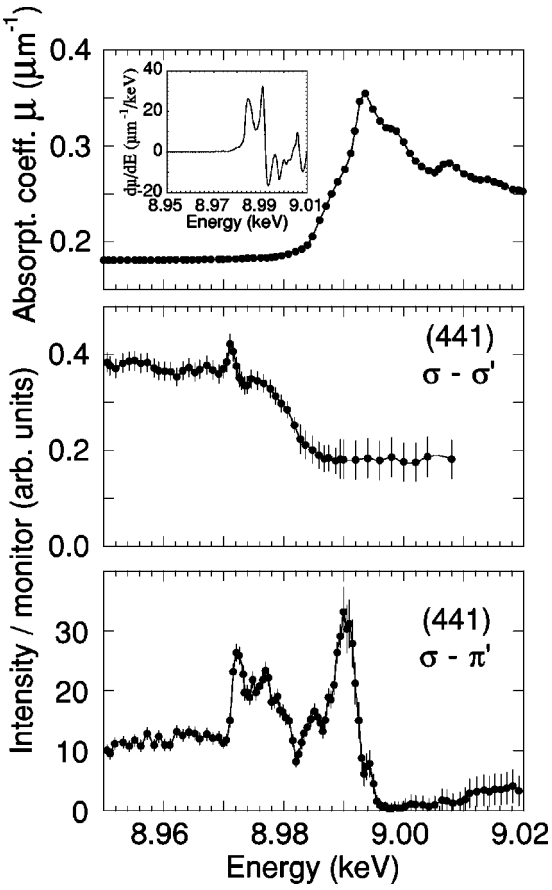

FIG. 2. Photon-energy dependence of the magnetic (441), integrated intensity near the Cu K-absorption edge. The upper panel shows the fluorescence and its energy derivative, as an energy reference. Data were collected at 12 K with both σ' (middle panel) and π' (lower panel) polarization of the scattered beam. Corrections for self-absorption have been applied, as stated in the text.

also in the σ-σ' spectrum. This indicates that the orbital angular momentum L gives a finite contribution to the Cu magnetic moment. Indeed, the intensity of AF-magnetic Bragg peaks is proportional to the square of the difference between the scattering amplitudes for the two sublattices. For the quadrupolar resonant term, this difference would vanish if the orbital moment of the atomic ground state was completely quenched,[31,32] as one would expect for Cu^{2+} in the first-order limit and octahedral symmetry. On the other hand, if $\langle L \rangle \neq 0$ the amplitude of the quadrupolar resonance in the σ-π' spectrum should increase with the modulus of the scattering vector. This expected behavior is confirmed by the data reported in Fig. 3, which shows the photon-energy dependence of the σ-π' integrated intensity for magnetic Bragg peaks with (0 0 l) Miller indices ($l = 1, 3, 5, 7$).

B. Nonresonant magnetic scattering

The non-resonant amplitude of magnetic scattering, $f_{nr}(Q)$, depends on the Fourier transform of the orbital and spin angular momentum densities, and allows a determination of the local orbital and spin moments. Quantitative information on the angular momentum contribution to the Cu

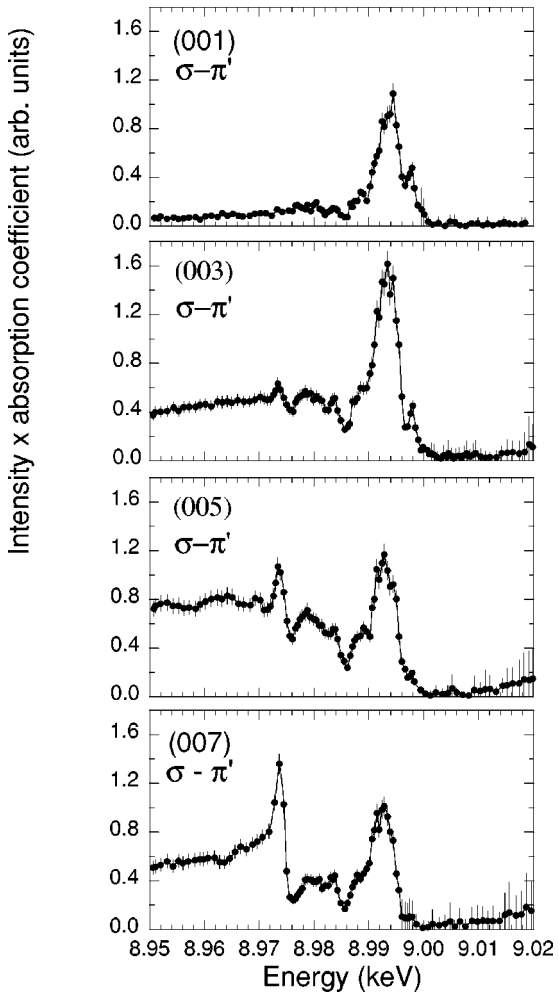

FIG. 3. Photon-energy dependence of the magnetic (001), (003), (005), and (007) integrated intensities near the Cu K-absorption edge. Data were collected at 12 K with π' polarization of the scattered beam, and corrected for self-absorption. The increase of the resonance amplitude at the quadrupolar threshold with the modulus of the scattering vector indicates a finite value of $\langle L \rangle$.

magnetic moment can therefore be obtained from measurements of integrated magnetic intensities far away from the resonance K edge.

Following Blume and Gibbs,[20] $f_{nr}(Q)$ for σ-σ' and σ-π' polarization channel can be written as

$$f_{nr}(Q) = \begin{bmatrix} f_{\sigma\text{-}\sigma'} \\ f_{\sigma\text{-}\pi'} \end{bmatrix} \propto \begin{bmatrix} \sin 2\theta \;\; S_2(\mathbf{Q}) \\ \sin\theta \sin 2\theta [S_1(\mathbf{Q}) + L_1(\mathbf{Q})] + 2\sin^3\theta S_3(\mathbf{Q}) \end{bmatrix}, \tag{1}$$

where θ is the Bragg angle, $\mathbf{Q} = \mathbf{k}_i - \mathbf{k}_f$ is the scattering vector, $S_i(\mathbf{Q})$ and $L_i(\mathbf{Q})$ are the components of the vector quantities $\mathbf{S}(\mathbf{Q})$ and $\mathbf{L}(\mathbf{Q})$ along the unit vectors $\mathbf{u}_i$ shown in Fig. 1 and defined in Ref. 20. $\mathbf{S}(\mathbf{Q})$ is the Fourier transform of the spin momentum density, while $\mathbf{L}(\mathbf{Q}=0)$ gives a measure of the orbital-moment magnetization.[20]

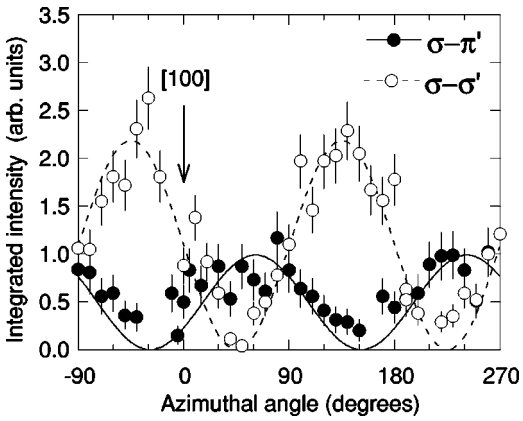

FIG. 4. Azimuthal scans about the (005) magnetic Bragg peak far away from resonance, at $T = 11$ K; closed circles correspond to the σ-π' channel, open circles to σ-σ'. Data points are intensities corrected for absorption. Lines are intensities calculated assuming magnetic moments along the [1 1 0] direction, for a collinear arrangement of spin and orbit moments.

Earlier studies suggested that the Cu spins in $KCuF_3$ are lying in the *a*-*b* plane, owing to the very weak *XY*-like anisotropy field that arises from dipolar and anisotropic exchange interaction.[12,33,34] With the [0 0 1] direction parallel to $\mathbf{u}_3$, the S_3 component is therefore zero, and Eq. (1) reduces to

$$f_{nr}(Q) \propto \begin{bmatrix} \sin 2\theta S \sin(\rho - \rho_S) \\ \sin\theta \sin 2\theta [S\cos(\rho - \rho_S) + L\sin(\rho - \rho_L)] \end{bmatrix}, \tag{2}$$

where ρ is the angle formed by the [1 0 0] direction and the $\mathbf{u}_1$ unit vector, ρ_S (ρ_L) is the angle between the [1 0 0] and the spin (orbital) moment direction.

The results of ρ (azimuthal) scans about the (005) magnetic peak, taken at $T = 11$ K with photon energy $\hbar\omega = 5.218$ keV, are shown in Fig. 4 for both the σ-σ' and the σ-π' channel. Intensities were calculated assuming them to be proportional to the square of the amplitudes given by Eqs. (2). Continuous lines in Fig. Fig. 4 show the calculated intensities, which are in agreement with collinear spin and orbit magnetic moments, lying along the [1 1 0] direction ($\rho_S = \rho_L = \pi/4$).

The ratio $L(Q)/S(Q)$ can be easily determined from scans similar to those reported in Fig. 4, as

$$\frac{L(Q)}{S(Q)} = \frac{\tan(\rho - \pi/4)}{\sin\theta} \sqrt{\frac{I_{\sigma\text{-}\pi'}}{I_{\sigma\text{-}\sigma'}}} - 1, \tag{3}$$

where $Q = 4\pi \sin\theta/\lambda$. The values obtained are shown in Fig. 5, the solid line being a fit of the data to the dipole approximation curve.[20] The extrapolation to $Q = 0$ gives $L/S = 0.29(5)$. Polarization analysis of nonresonant magnetic scattering[35] and LDA+U calculations[36] have given comparable values of L/S for Ni in NiO. This result implies either a reduced symmetry at the Cu sites, e.g., that suggested in Ref. 6, or a mixing with excited states.

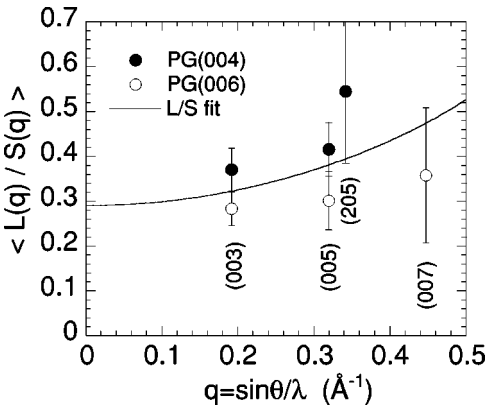

FIG. 5. The $L(Q)/S(Q)$ ratio as a function of $q=Q/4\pi$, as deduced from the nonresonant azimuthal scans. Data have been collected at two different incident photon energies (5.218 and 7.828 keV) using pyrolitic graphite (004) and (006) polarization analyzers, respectively. The solid line is a fit to the dipolar model described by Blume and Gibbs. Extrapolation to $Q=0$ gives an estimate of the orbital contribution to the Cu magnetic moment.

IV. ORBITAL ORDERING

Resonant superlattice reflections corresponding to a propagation vector $\langle 111\rangle$ indicate the presence of long-range $3d$ orbital order in the *type-a* structure. Much weaker structurally forbidden peaks with propagation vector $\langle 110\rangle$, corresponding to orbital ordering within the small amount of *type-d* variant present in the samples, were also visible.

Figure 6 shows, as an example, the energy dependence of the σ-π' integrated intensity for the (331) (*type a*) and for the (330) (*type d*) Bragg peaks. The enhancement of the intensity of orbital superlattice reflections occurs only about the dipole threshold energy, which identifies the resonance with $1s\rightarrow 4p$ transitions.

When the crystal is rotated around the scattering vector at the dipole resonance, the orbital σ-π' superlattice peaks exhibit a characteristic oscillation with twofold symmetry. The azimuthal angle dependence of the (331) orbital peak is shown in Fig. 7, and compared with the azimuthal intensity oscillation of the (005) magnetic intensity, measured at the same energy (8.992 keV) and temperature (12 K). The solid lines in Fig. 7 are fits to the square of the sinusoidal function, $\sin^2(\rho+\alpha)$. In drawing the figure, the origin of the (005) azimuthal scan has been set to the orientation where the incident polarization vector is parallel to [100], whilst for the (331) scan $\rho=0$ corresponds to the incident polarization vector parallel to [001]. The results obtained show that the orbital and magnetic azimuthal scans are shifted by $\Delta\alpha=\pi/4$. This is a direct proof that the Cu magnetic moments, whose direction in the $a-b$ plane has been a subject of controversy, are directed along the [110] direction of the pseudocubic perovskite cell, whilst the main contribution to the orbital signal comes from the difference in $p_{x(y)}$ density of states on the two sublattices.[28] The relative arrangement of occupied orbitals and magnetic-moment directions is shown in Fig. 8.

Figure 9 shows the integrated intensity of the σ-π' magnetic (441) and orbital (331) Bragg reflections as a function of temperature. As the temperature is lowered, no variations

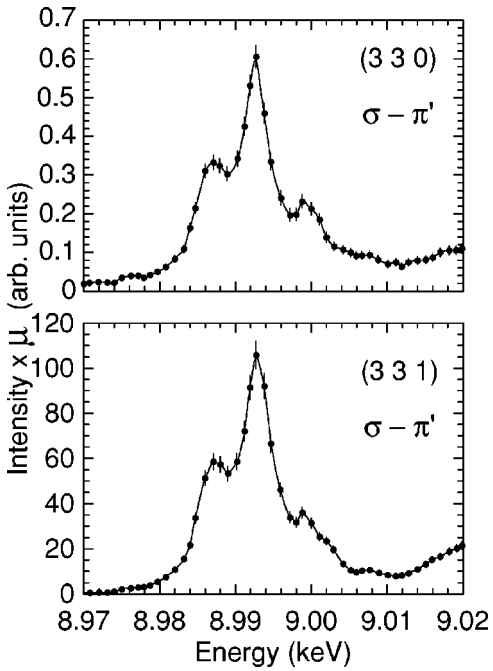

FIG. 6. Energy dependence of σ-π' intensities of the (330) and (331) superlattice reflections, corresponding to long-range ordering of $3d$ Cu orbitals in the *type-d* and *type-a* variants of $KCuF_3$. Data were recorded at 12 K, and are corrected for absorption.

are observed for the charge peaks, neither in intensity nor in position and width. On the other hand, the intensity of the orbital peaks, which is practically constant down to 43 K, does increase below this temperature and saturates below 38 K, where the magnetic order starts to develop. A similar increase in intensity of the orbital peaks, in a temperature region where the orbital order parameter (OP) Ψ is expected to be saturated, has been reported near T_N for several manganites.[22,24,37]

V. LSDA AND LSDA+*U ab initio* CALCULATIONS

Although electronic correlations in the narrow band $3d$ subsystem can only partly be described within the local-

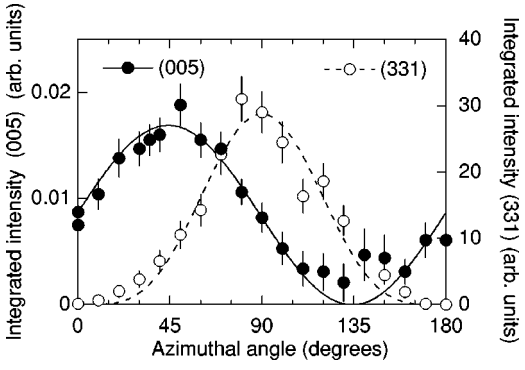

FIG. 7. Azimuthal angle dependence of the magnetic (005) (closed circles) and the orbital (331) (open circles) σ-π' intensities. Data were taken at 12 K, with incident energy of 8.992 keV and LiF(004) analyzer. The solid lines are the twofold squared sinusoidal curve describing the angular dependence.

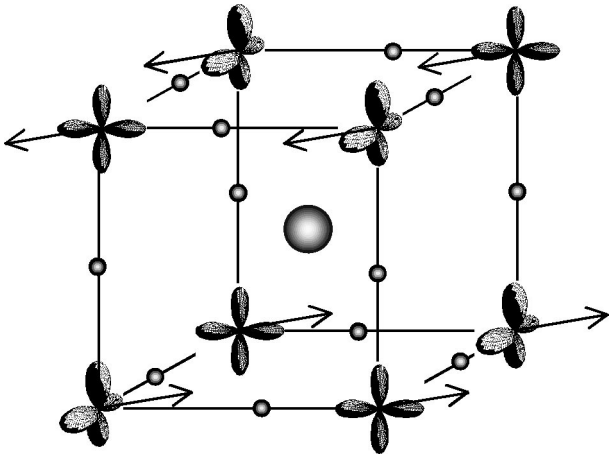

FIG. 8. The *type a* crystal structure of $KCuF_3$. A possible ordered pattern of the Cu $3d$ orbitals is schematically shown. The large circle represents the K ions, the small, full circles are the F ions. The arrows indicate the direction of the magnetic moments in the ordered phase.

density approximation of the density-functional theory, this approach does give reliable results for the wide bands formed by the $4p$ states. We calculate the electronic structure of $KCuF_3$ with the linear muffin-tin orbital method within the atomic sphere aproximation (LMTO-ASA) LSDA method[38] using the LMTO47 Stuttgart code and with the LSDA$+U$ extension of this method,[39] which incorporates a mean-field treatment of the strong correlations in the e_g subsystem. The calculations are performed for the crystallographic *a*-type structure of $KCuF_3$ (Ref. 40) and the Coulomb and exchange parameters are $U=7.5$ eV and $J=0.9$ eV, equal to the values of Liechtenstein *et al.*[7] in their calculation for the *d*-type structure of $KCuF_3$.

Our LSDA calculation ($U=J=0$) produces a paramagnetic metallic ground state for $KCuF_3$ (as in Refs. 7,41), which indicates that in this system the Jahn-Teller distortion is not so strong that it can induce a bandgap. In $LaMnO_3$, which is an e_g orbital ordered system as well, the Jahn-Teller distortion is apparently stronger: from band-structure calculations one finds that the Jahn-Teller splitting between e_g orbitals induces a bandgap of 278 meV for the manganite.[42] For $KCuF_3$ we can compare the energy difference between the first moment of the two e_g partial occupied densities of states, which we find to be 132 meV, with the Jahn-Teller energy calculated in Ref. 43, where $E_{JT}=120$ meV and 177 meV were found with two different computational methods. The Jahn-Teller energy for the cuprate is thus approximately half of the Jahn-Teller energy for the undoped manganite.

From our LSDA$+U$ calculation we find a ground state with *a*-type orbital order of alternating $d_{y^2-z^2}$ and $d_{x^2-z^2}$ orbitals, shown in Fig. 8, and a charge gap of 2.47 eV, which is somewhat larger than the gap of 2 eV found for the *d*-type structure,[7] but smaller than the gap found in an unrestricted Hartree-Fock approach.[43] The calculation also gives the correct magnetic order. It is therefore the electron-electron interaction in the e_g subsystem, which induces the large single particle excitation gap in $KCuF_3$.

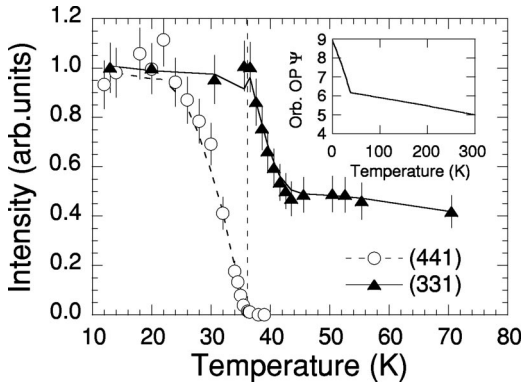

FIG. 9. Temperature dependence of the integrated intensity of the (331) orbital ordering peak (triangles) and the magnetic (441) Bragg reflection (circles). The qualitative behavior of the orbital order parameter Ψ as a function of temperature, computed in the mean-field approximation described in the text, is shown in the inset.

VI. DISCUSSION

It is generally believed that in the RXS experiment an electron makes a dipolar transition, in this case from a Cu $1s$ to $4p$ state, as higher-order transitions have much smaller cross sections.[27] Different Cu $3d$ orbitals with e_g symmetry are occupied on different sublattices—the orbital order—and corresponding to this reduced translation symmetry extra Bragg reflections can appear if the orbital order of the *d* states is somehow reflected in an electronic inequivalence of the Cu $4p_x$, p_y and/or p_z states. In the approach of Ishihara *et al.*[44,45] the intra-atomic Coulomb interaction between the Cu $3d$ and $4p$ states gives rise to the splitting of the *p* levels. Elfimov *et al.*[26] pointed out, however, that as the orbital order of the e_g electrons couples to the lattice via the Jahn-Teller effect, the resulting lattice distortion in turn splits the $4p$ states. As the *p* states are delocalized—their bandwidth is in the order of 10 eV—one needs to generalize the RXS cross section to a band-structure framework.[28] It is this computational scheme that we adopt here. For additional details about the adopted method see Ref. 28.

The Cu K-edge resonance spectra that we obtain from the band-structure calculation are shown in Fig. 10, where we used a broadening of $\tau^{-1}=1.5$ eV due to the core-hole lifetime.[26] The spectrum consists of two main peaks, where the low-energy peak has less intensity. Note that the energy scale in the calculation is relative to the chemical potential as it does not include the core-hole energy. Comparing the calculations for $U=0$ and $U=7.5$ eV, we see that the spectra have roughly the same structure, be it that the $U=7.5$ eV spectrum is shifted to higher energy and that in this case the low-energy peak has somewhat smaller spectral weight. The shift of the spectrum is due to the opening of a gap at the Fermi level. The resemblance of the two spectra shows that the RXS intensity is for the largest part determined by the Jahn-Teller distortion and that the Coulomb interactions among the $3d$ states only play a minor role for the RXS signal. This is in contrast to the electronic gap in $KCuF_3$,

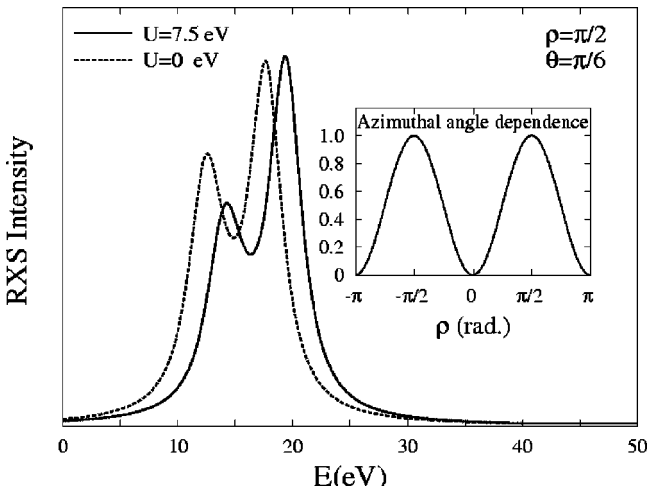

FIG. 10. Total calculated resonant x-ray intensity for the (331) orbital superlattice reflection on the Cu K edge, with and without on-site Coulomb interaction U. In the inset the azimuthal angle dependence of the signal is shown for fixed polar angle θ.

which is mostly determined by electron correlations and has little Jahn-Teller contribution.

We also calculate the azimuthal angle (ρ) dependence of the RXS resonance and find an almost perfect $\sin^2\rho$ behavior, shown in the inset of Fig. 10, as one would expect because the CuF_6 octahedra are not tilted.[28] In Fig. 11 the experimental and calculated spectra are directly compared and we see that there is a remarkable agreement. The high-energy shoulder around $E=25$ eV (on the energy scale of Fig. 11) is absent in the theoretical result, but the splitting of the two main peaks and their relative intensities are correctly given

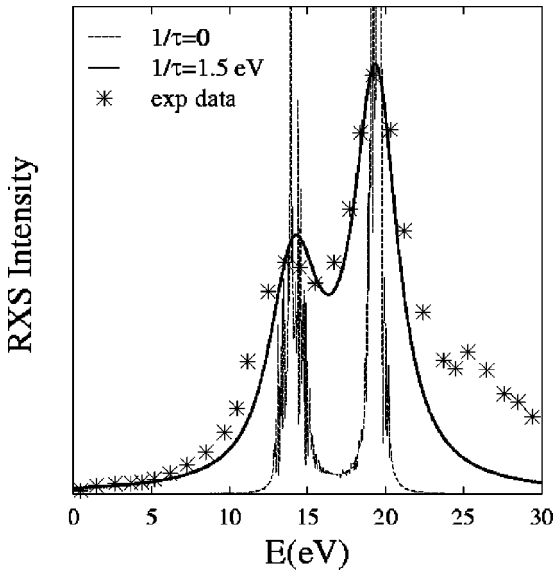

FIG. 11. Resonant x-ray spectrum for the (331) reflection on the Cu K edge. Thin line represents the LSDA+U result, without core-hole broadening ($\tau^{-1}=0$), thick line represents the LSDA+U result with $\tau^{-1}=1.5$ eV, the asterisks represent the experimental results. The experimental data are shown relative to the core-hole energy of 8973.5 eV.

by our *ab initio* band-structure calculation. This is an indication of the reliability of band-structure methods for describing and predicting resonant x-ray spectra and at the same time an indication that resonant x-ray intensities in transition- metal oxides reflect the e_g orbital order parameter via the Jahn-Teller lattice deformation.[26,28,46]

An interesting result of the present experiments is given by the temperature variation of the intensity of orbital-order peaks, increasing to a larger saturation value when the temperature decreases below the magnetic ordering point.

Ishihara and Maekawa[47] suggest that this anomalous temperature dependence signals a change in the type of orbital order near the magnetic transition. In particular, an intensity increase is expected if the orbital state changes from a $d_{z^2-x^2}$-$d_{z^2-y^2}$ type of order to a state where $d_{z^2-x^2(z^2-y^2)}$ orbitals are hybridized with $d_{3x^2-r^2(3y^2-r^2)}$ orbitals. In the present case, however, we note that no variation in the JT distortion of the fluorine octahedra is observed around T_N.

An alternative model that account for the behavior of the orbital OP vs temperature, as measured by x-ray scattering in $KCuF_3$ and in the transition-metal oxides, is described below. The basic physical idea is that the magnetic order is driven by the orbital order, in the sense that the exchange constants between spins of neighboring atoms are determined by the relative orientation of the occupied orbitals on these atoms, as summarized by the Goodenough-Kanamori-Anderson model.

We can try to model the interplay of Ψ, the orbital OP, and S, the magnetization OP, by writing a simple Landau effective free energy F, which acknowledges that the magnetic critical temperature is determined by the exchange constants and that those are in turn related to the orbital OP, which we take constant throughout the volume. We assume that the Néel temperature is proportional to Ψ^2, which is the simplest form of dependence,

$$F=a_1(T-T_{OO})\Psi^2+b_1\Psi^4+a_2(T-a_2'\Psi^2)S^2+b_2S^4, \tag{4}$$

where all the a's and b's are positive, real constants, the only restriction being that $4b_1b_2-a_2^2a_2'^2>0$, to ensure that F has a lower bound. At high temperature, $T>T_{OO}$, both Ψ and S are zero. As T becomes smaller than T_{OO}, Ψ begins to grow, according to the mean-field law,

$$\Psi^2(T)=\frac{a_1(T_{OO}-T)}{2b_1}. \tag{5}$$

However, S remains vanishing until a temperature T_N is reached such that $T_N=a_2'\Psi^2(T_N)$, which means

$$T_N=\frac{a_2'a_1T_{OO}}{2b_1+a_2'a_1}. \tag{6}$$

For $T<T_N$, also S is nonvanishing, therefore the equation determining Ψ is modified. In fact, the minimization of the free energy with respect to both OP gives

$$dF/d\Psi^2 = a_1(T - T_{OO}) + 2b_1\Psi^2 - a_2' a_2 S^2 = 0,$$

$$dF/dS^2 = a_2(T - a_2'\Psi^2) + 2b_2 S^2 = 0, \tag{7}$$

and consequently for $T < T_N$,

$$\Psi^2 = \frac{2b_2 a_1 \left[T_{OO} - \left(1 + \frac{a_2^2 a_2'}{2a_1 b_2} \right) T \right]}{4b_1 b_2 - a_2^2 a_2'^2}, \tag{8}$$

which corresponds to a steeper rise and a larger saturation value of the orbital OP as the temperature further decreases below T_N. Adjusting the parameters so that $T_{OO} \simeq 800$ K, $T_N \simeq 38$ K, and saturation values are comparable to experiment, it is easy to generate a behavior of Ψ similar to the observed one, as shown in the inset of Fig. 9.

VII. CONCLUSIONS

Resonant x-ray scattering experiments on $KCuF_3$ have given new information on the magnetic ordered state of this system and have shown that the magnetic and the $3d$ orbital order are closely related, even though the associated energy scales differ by more than a factor of 20. Both resonant and nonresonant magnetic scattering measurements point to a non-negligible orbital contribution to the total magnetic moment of the Cu ions. From nonresonant measurements it is clear that the orbital and spin part of the Cu magnetic moment are collinear and directed along the [1 1 0] direction, the ratio L/S being close to 0.3. The orbital ordering results in the appearance of forbidden Bragg reflections corresponding to the $\langle 110 \rangle$ propagation vector. These reflections show a strong resonant enhancement for x-ray energies close to the Cu $1s \rightarrow 4p$ transition, and are therefore better ascribed to a difference in the $p_{x(y)}$ density of states. LSDA and LSDA $+U$ calculations give a large value for the single particle excitation gap, induced by the electron-electron interaction in the e_g subsystem, the Jahn-Teller contribution being almost negligible. On the other hand, it is the Jahn-Teller distortion that essentially determines the RSX intensity, the Coulomb interaction between the $3d$ electrons playing a minor role. A sudden increase of the orbital order parameter is found in the temperature range close to (but slightly higher than) the Néel temperature. This increase is indicative of a strong coupling between the orbital and the magnetic order parameters, in agreement with the Goodenough-Kanamori-Anderson rules, in the sense that the orbital occupancy determines the sign and value of the exchange constants. This last result can be interpreted in the light of a semiquantitative model that gives a trend with temperature of the orbital order parameter that is reasonably comparable with the experimental results. As a final remark, we can note that the proposed model can explain similar experimental results found in the colossal magnetoresistance (CMR) manganites, thus questioning the interpretation that ascribes them to a change in the orbital ordered state.

ACKNOWLEDGMENTS

We thank the ID20 team at ESRF for valuable help during the experiments, and G.H. Lander, C. Vettier, and I.S. Elfimov for stimulating discussions.

[1] J.B. Goodenough, *Magnetism and the Chemical Bond* (Interscience, New York, 1963).
[2] K.I. Kugel' and D.I. Khomskii, Zh. Eksp. Teor. Fiz. **64**, 1429 (1973) [Sov. Phys. JETP **37**, 725 (1973)].
[3] K.I. Kugel' and D.I. Khomskii, Usp. Fiz. Nauk **136**, 621 (1982) [Sov. Phys. Usp. **25**, 231 (1982)].
[4] A.M. Oleś, L.F. Feiner, and J. Zaanen, Phys. Rev. B **61**, 6257 (2000).
[5] L.F. Feiner, A.M. Oleś, and J. Zaanen, Phys. Rev. Lett. **78**, 2799 (1997).
[6] M. Hidaka, T. Eguchi, and I. Yamada, J. Phys. Soc. Jpn. **67**, 2488 (1998).
[7] A.I. Liechtenstein, V.I. Anisimov, and J. Zaanen, Phys. Rev. B **52**, R5467 (1995).
[8] S.K. Satija, J.D. Axe, G. Shirane, H. Yoshizawa, and K. Hirakawa, Phys. Rev. B **21**, 2001 (1980).
[9] D.A. Tennant, T.G. Perring, R.A. Cowley, and S.E. Nagler, Phys. Rev. Lett. **70**, 4003 (1993).
[10] D.A. Tennant, R.A. Cowley, S.E. Nagler, and A.M. Tsvelik, Phys. Rev. B **52**, 13 368 (1995).
[11] D.A. Tennant, S.E. Nagler, D. Welz, G. Shirane, and K. Yamada, Phys. Rev. B **52**, 13 381 (1995).
[12] M.T. Hutchings, E.J. Samuelsen, G. Shirane, and K. Hirakawa, Phys. Rev. **188**, 919 (1969).
[13] B. Lake, D.A. Tennant, and S.E. Nagler, Phys. Rev. Lett. **85**, 832 (2000).
[14] J.P. Hannon, G.T. Trammell, M. Blume, and D. Gibbs, Phys. Rev. Lett. **61**, 1245 (1988); **62**, 2644(E) (1989).
[15] P. Carra and B.T. Thole, Rev. Mod. Phys. **66**, 1509 (1994).
[16] J.P. Hill and D.F. McMorrow, Acta Crystallogr., Sect. A: Found. Crystallogr. **52**, 236 (1996).
[17] E.N. Ovchinnikova and V.E. Dmitrienko, Acta Crystallogr., Sect. A: Found. Crystallogr. **56**, 2 (2000).
[18] J.I. Igarashi and M. Takahashi, Phys. Rev. B **63**, 184430 (2001).
[19] M. Blume, J. Appl. Phys. **57**, 3615 (1985).
[20] M. Blume and D. Gibbs, Phys. Rev. B **37**, 1779 (1988).
[21] Y. Murakami, H. Kawada, H. Kawata, M. Tanaka, T. Arima, Y. Moritomo, and Y. Tokura, Phys. Rev. Lett. **80**, 1932 (1998).
[22] Y. Murakami, J.P. Hill, D. Gibbs, M. Blume, I. Koyama, M. Tanaka, H. Kawata, T. Arima, Y. Tokura, K. Hirota, and Y. Endoh, Phys. Rev. Lett. **81**, 582 (1998).
[23] Y. Endoh, K. Hirota, S. Ishihara, S. Okamoto, Y. Murakami, A. Nishizawa, T. Fukuda, H. Kimura, H. Nojiri, K. Kaneko, and S. Maekawa, Phys. Rev. Lett. **82**, 4328 (1999).
[24] M.v. Zimmermann, J.P. Hill, D. Gibbs, M. Blume, D. Casa, B. Keimer, Y. Murakami, Y. Tomioka, and Y. Tokura, Phys. Rev. Lett. **83**, 4872 (1999).
[25] L. Paolasini, C. Vettier, F. de Bergevin, F. Yakhou, D. Mannix, A.

Stunault, W. Neubeck, M. Altarelli, M. Fabrizio, P.A. Metcalf, and J.M. Honig, Phys. Rev. Lett. **82**, 4719 (1999).
[26] I.S. Elfimov, V.I. Anisimov, and G.A. Sawatzky, Phys. Rev. Lett. **82**, 4264 (1999).
[27] M. Benfatto, Y. Joly, and C.R. Natoli, Phys. Rev. Lett. **83**, 636 (1999).
[28] P. Benedetti, J. van den Brink, E. Pavarini, A. Vigliante, and P. Wochner, Phys. Rev. B **63**, 060408(R) (2001).
[29] A. Stunault, C. Vettier, F. de Bergevin, N. Bernhoeft, V. Fernandez, S. Langridge, E. Lidström, J.E. Lorenzo-Diaz, D. Wermeille, L. Chabert, and R. Chagnon, J. Synchrotron Radiat. **5**, 1010 (1998).
[30] K. Hirakawa and Y. Kurogi, Suppl. Prog. Theor. Phys. **46**, 147 (1970).
[31] S.W. Lovesey, J. Phys.: Condens. Matter **10**, 2505 (1998).
[32] S.W. Lovesey, O. Fritz, and E. Balcar, J. Phys.: Condens. Matter **10**, 501 (1998).
[33] H. Kubo, F. Tanaka, N. Kaneshima, and K. Hirakawa, Solid State Commun. **18**, 79 (1976).
[34] S. Sasaki, N. Narita, and I. Yamada, J. Phys. Soc. Jpn. **64**, 4882 (1995).
[35] V. Fernandez, C. Vettier, F. de Bergevin, C. Giles, and W. Neubeck, Phys. Rev. B **57**, 7870 (1998).
[36] S.K. Kwon and B.I. Min, Phys. Rev. B **62**, 73 (2000).
[37] Y. Wakabayashi, Y. Murakami, I. Koyama, T. Kimura, Y. Tokura, Y. Moritomo, K. Hirota, and Y. Endoh, J. Phys. Soc. Jpn. **69**, 2731 (2000).
[38] O.K. Andersen and O. Jepsen, Phys. Rev. Lett. **53**, 2571 (1984).
[39] V.I. Anisimov, J. Zaanen, and O.K. Andersen, Phys. Rev. B **44**, 943 (1991).
[40] R.H. Buttner, E.N. Maslen, and N. Spadaccini, Acta Crystallogr., Sect. B: Struct. Sci. **46**, 131 (1990).
[41] V. Eyert and K.H. Hock, J. Phys.: Condens. Matter **5**, 2987 (1993).
[42] P. Ravindran, A. Kjekshus, H. Fjellvåg, A. Delin, and O. Eriksson, Phys. Rev. B **65**, 064445 (2002).
[43] M.D. Towler, R. Dovesi, and V.R. Saunders, Phys. Rev. B **52**, 10 150 (1995).
[44] S. Ishihara and S. Maekawa, Phys. Rev. Lett. **80**, 3799 (1998).
[45] S. Ishihara and S. Maekawa, Phys. Rev. B **58**, 13 442 (1998).
[46] M. Takahashi, J. Igarashi, and P. Fulde, J. Phys. Soc. Jpn. **68**, 2530 (1999).
[47] S. Ishihara and S. Maekawa, Phys. Rev. B **62**, R9252 (2000), and references therein.